Three-Dimensional Structure of Wind Turbine Wakes as Measured by Scanning Lidar

Nicola Bodini[1,2], Dino Zardi[2], and Julie K. Lundquist[1,3]

[1]Department of Atmospheric and Oceanic Sciences, University of Colorado Boulder, Boulder, Colorado, USA
[2]Department of Civil, Environmental and Mechanical Engineering, University of Trento, Trento, Italy
[3]National Renewable Energy Laboratory, Golden, Colorado, USA

Correspondence to: Nicola Bodini (nicola.bodini@colorado.edu)

Abstract. The slower wind speeds and increased turbulence that are characteristic of turbine wakes have considerable consequences on large wind farms: turbines located downwind generate less power and experience increased turbulent loads. The structures of wakes and their downwind impacts are sensitive to wind speed and atmospheric variability. Wake characterization can provide important insights for turbine layout optimization in view of decreasing the cost of wind energy. The CWEX-13 field campaign, which took place between June and September 2013 in a wind farm in Iowa, was designed to explore the interaction of multiple wakes in a range of atmospheric stability conditions. Based on lidar wind measurements, we extend, present, and apply a quantitative algorithm to assess wake parameters such as the velocity deficits, the size of the wake boundaries, and the location of the wake centerlines. We focus on wakes from a row of four turbines at the leading edge of the wind farm to explore variations between wakes from the edge of the row (outer wakes) and those from turbines in the center of the row (inner wakes). Using multiple horizontal scans at different elevations, a three-dimensional structure of wakes from the row of turbines can be created. Wakes erode very quickly during unstable conditions, and can in fact be detected primarily in stable conditions in the conditions measured here. During stable conditions, important differences emerge between the wakes of inner turbines and the wakes of outer turbines. Further, the strong wind veer associated with stable conditions results in a stretching of the wake structures, and this stretching manifests differently for inner and outer wakes. These insights can be incorporated into low-order wake models for wind farm layout optimization or for wind power forecasting.

1 Introduction

A wind turbine wake is the volume downwind of a wind turbine, affected by the fact that the wind turbine removes momentum from the flow, thus reducing the downwind speed. In this wake, the flow is more turbulent than in the inflow, because of the rotation of turbine blades and the presence of the wind turbine itself as an obstacle to the incoming wind flow (Landberg, 2015).

Wind turbine wakes impact the layout optimization and energy production of large wind farms (Brower, 2012). In fact, the reduced wind speed in the wake region has a direct effect on the generation of power by downwind turbines (Spera, 1985; Nygaard, 2014). Barthelmie et al. (2010) found up to a 40% reduction in the power generated by turbines in wakes as compared

to leading-edge or unwaked turbines. Moreover, the increased turbulence in wakes enhances turbulent loads for downwind turbines, possibly inducing premature failure (Crespo et al., 1999; Sathe et al., 2013).

Therefore, wakes need to be studied and understood in order to maximize the efficiency of wind energy production. In particular, wake models are applied in several steps of the design and life-time management of wind farms: layout of wind farms

5   is studied in detail, in order to maximize the amount of energy generated by the turbines (Elkinton et al., 2006; Samorani, 2013). Moreover, the overall wind resource assessment process needs to take into account the effect of wakes to have a reliable prediction of future power production (Brower, 2012; Clifton et al., 2016). Lastly, wind farm control techniques incorporate detailed studies of wake characteristics while periodically changing some features of the turbines (such as yaw angle and pitch angle) in order to maximize the overall power production from the whole wind farm (Fleming et al., 2014, 2016; Gebraad

10 et al., 2016; Vollmer et al., 2016b). Typically, all these processes are computationally intensive, and apply low-order models of turbine wakes (Elkinton et al., 2006; Chowdhury et al., 2012), such as the Jensen model (Jensen et al., 1984). In this way, several scenarios can be tested, but these lower-cost models oversimplify reality and may not be capable to fully represent wake characteristics in a detailed and realistic way (Barthelmie et al., 2006; Andersen et al., 2014).

Atmospheric stability has been shown to have a major impact on wind turbine wake evolution and wind farm performance in

15 both observational (Magnusson and Smedman, 1994; Hansen et al., 2012; Wharton and Lundquist, 2012; Vanderwende and Lundquist, 2012; Barthelmie et al., 2013; Dörenkämper et al., 2015; Machefaux et al., 2015; Mirocha et al., 2015) and modeling studies (Churchfield et al., 2012; Aitken et al., 2014b; Mirocha et al., 2014; Machefaux et al., 2015; Abkar and Porté-Agel, 2015; Abkar et al., 2015): wakes in stable conditions persist for long distances downwind, while during unstable conditions the enhanced turbulent mixing erodes the wakes more quickly.

20 Wake characterization from field data can validate and improve the quality of numerical models. Data from field campaigns avoid possible limitations of wind tunnel simulations, such as down-scaled geometric dimensions and low Reynolds number (Iungo et al., 2013). Lidars and radars have been widely used recently to characterize wind turbine wakes. These instruments can measure wind characteristics above the heights of most traditional meteorological towers, and they can be deployed and moved rather easily, allowing measurements at several different locations. Many wake validation studies from remote sensing

25 measurements focus on individual isolated turbines (Käsler et al., 2010; Bingöl et al., 2010; Trujillo et al., 2011; Hirth et al., 2012; Hirth and Schroeder, 2013; Aitken et al., 2014a; Aitken and Lundquist, 2014; Bastine et al., 2015; Kumer et al., 2015), with some studies that aim at reconstructing the 3-dimensional structure of wind turbine wakes (Iungo et al., 2013; Banta et al., 2015). The interactions between multiple wakes must be captured in studies of large wind farms: see Clive et al. (2011); Aubrun et al. (2016) among others.

30 In this paper, we analyze scanning lidar and profiling lidar measurements from the CWEX-13 field campaign in a large wind farm in Iowa, and we extend the individual wake detection algorithm proposed by Aitken et al. (2014a) to characterize multiple wakes. The three-dimensional structure of wakes from a row of four turbines is assessed, in terms of velocity deficit, width of the wakes, and wake centerlines. Section 2 describes the CWEX-13 field campaign and how we use measurements from the instruments deployed at the site. In Section 3 we present the wake characterization algorithm for multiple wakes, an expansion

35 of the algorithm proposed by Aitken et al. (2014a). Section 4 highlights how wake characteristics (velocity deficit, wake width,
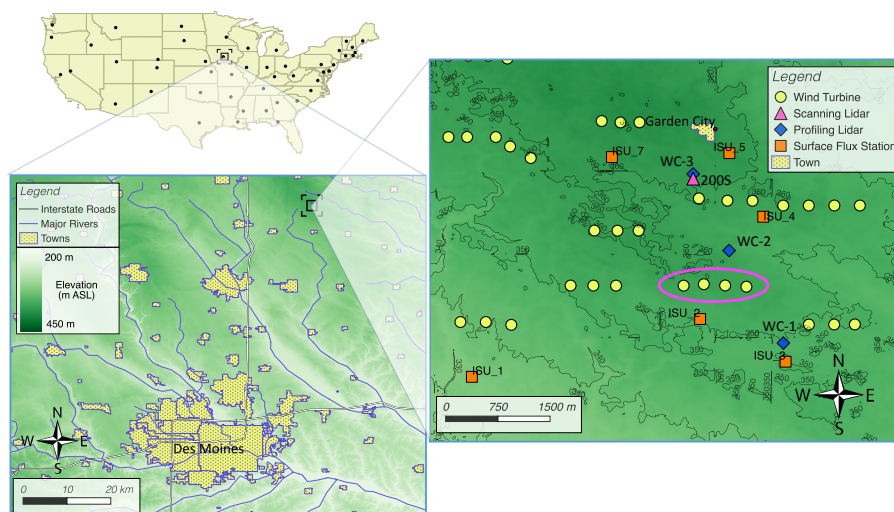
Figure 1. Schematic view of the part of the wind farm in central Iowa where the CWEX-13 field campaign took place. The row of 4 turbines whose wakes are detected by the scanning lidar is highlighted in a purple ellipse.

and wake centerline) change in three-dimensional space, and for the first time we quantify the effect of ambient wind veer on the vertical stretching of the structure of wakes. In Section 5 we compare the present results with those obtained in previous studies, and we suggest possible future work to improve wake simulations and models.

2 Data and Methods

5 This study analyzes the scanning lidar and profiling lidar measurements from the CWEX-13 observational campaign, summarized in Takle et al. (2014) and Vanderwende et al. (2015).

2.1 CWEX-13 Observational dataset

CWEX-13 campaign (Lundquist et al., 2014) took place between late June and early September 2013 in a wind farm in central Iowa, the same wind farm studied in previous CWEX campaigns; however, CWEX-13 focused on a part of the wind farm that

10 is different from what is discussed in Rajewski et al. (2013), Rhodes and Lundquist (2013), Mirocha et al. (2015), and Lee and Lundquist (2017). The region exhibits strong diurnal cycles of atmospheric stability, and frequent nocturnal low-level jets (Vanderwende et al., 2015). The area has a flat topography, with large fields of corn (height $1 - 2$ m) and soybeans (height $0.3 - 0.8$ m). The region also has four small villages, some riparian regions, and a few trees and buildings.

Figure 1 shows a schematic diagram of the area of the wind farm of interest in CWEX-13. The yellow dots represent the

15 wind turbines, whose main technical specifications are reported in Table 1. For the purpose of this work, we focus on the characterization, using scanning lidar data, of the wakes from the row of 4 turbines enclosed in the purple ellipse in Figure 1.

Table 1. Technical specifications of the studied wind turbines in CWEX-13 field campaign.

Rotor diameter (D)	80 m
Hub height	80 m
Rated power	1.5 MW
Cut-in wind speed	3.5 m s^{-1}
Rated power at	11 m s^{-1}
Cut-out wind speed	20 m s^{-1}

2.1.1 Lidar measurements

As shown by the scheme in Figure 1, three vertical profiling lidars and a scanning lidar were deployed at the site during the field campaign. Three WINDCUBE v1 vertical profiling lidars (blue diamonds in Figure 1) were located south of the studied row of four turbines, $8.5D$ north of the above-mentioned turbines, and $5.7D$ north of a second row of turbines. These instruments

5   provided vertical profiles of wind speed and direction from 40 m to 220 m above the surface, with measurements collected every 20 m.

From 31 July to 6 September 2013, a LEOSPHERE WINDCUBE 200S scanning lidar was deployed with the northernmost WINDCUBE v1 profiling lidar (WC-3 in Figure 1). Vanderwende et al. (2015) demonstrated good agreement between the co-located scanning and profiling lidars measurements at the altitudes where measurements overlapped. Scanning lidars can

10   operate sweeping the azimuth angle with a constant elevation angle, the so-called *plan-position-indicator* (PPI) mode, or sweeping the elevation angle while holding the azimuth angle fixed, in the so-called *range-height-indicator* (RHI), mode (Sathe and Mann, 2013). In CWEX-13, the scanning lidar used a combination of both PPI and RHI scans, with a 30-minute cycle. Measurements were collected with slant range gates of 50 m at ranges up to 5000 m from the instrument, with an angular resolution of $0.1°$. Line-of-sight (radial) velocity was measured with an accuracy better than 0.5 m s^{-1}

15   . At CWEX-13, southerly wind conditions dominated the campaign. Thus, the WINDCUBE 200S scanning lidar can use horizontal (PPI) scans, to observe wakes propagating from the row of four turbines of interest. The horizontal scans were performed at six different elevation angles, giving a range of different vertical positions depending on the distance from the lidar. Elevation angles varied from $1.5°$ to $2.8°$, which allow measurements at a variety of vertical positions between the bottom and top of the rotor disk of the turbines, as shown in Figure 2.

20   We select for a detailed analysis two days (23 and 26 August 2013) displaying wind conditions representative of the typical southerly wind pattern for the site. The first case, 23 August, had predominant southeasterly wind conditions, with relatively low wind speed, which never exceeded 10 m s^{-1} at 220 m AGL. During 23 August 2013, 438 PPI scans were performed, 73 for each of the 6 elevation angles. On the other hand, 26 August showed southwesterly wind, which is the most common situation for the site, with greater wind speed (up to 20 m s^{-1} at 220 m AGL). During 26 August 2013, 576 PPI scans were performed,
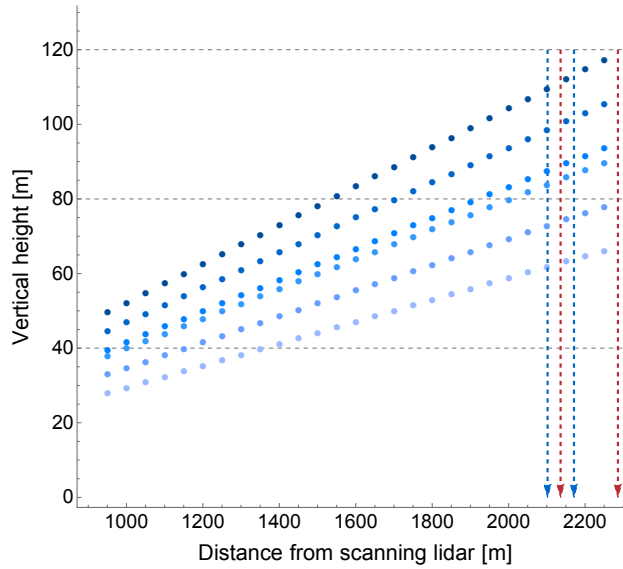
Figure 2. Schematic representation of the position where measurements from PPI scans are available, at 6 different elevation angles, as a function of the distance from the scanning lidar. The horizontal dashed lines show the vertical limits of the rotor disk of the turbines and hub height. The position of the 4 turbines is represented by the vertical dashed lines, with red lines for outer turbines and blue lines for inner turbines. The change in elevation between the turbine location and the lidar location is taken into account.

96 for each elevation angle. By comparing the results from these two different days, the effect of wind direction on some wake characteristics can be assessed.

2.1.2 Surface flux measurements for quantifying atmospheric stability

Several surface flux stations (provided by Iowa State University) were deployed at the CWEX-13 site (orange squares in
5 Figure 1). Measurements from surface flux stations can be used to assess atmospheric stability conditions, with the calculation of Obukhov length L, defined as:

$$L = -\frac{\overline{\theta_v} \cdot u_*^3}{k \cdot g \cdot \overline{w'\theta_v'}} \quad (1)$$

where θ_v is the virtual potential temperature (K), calculated from the sonic anemometer virtual temperature data T_v and the measured pressure p as $\theta_v = T_v \left(\frac{p_0}{p}\right)^{R/c_p}$ with $p_0 = 1000$ hPa, and $R/c_p \approx 0.286$; $k = 0.4$ is the von Kármán constant;
10 $g = 9.81$ m s^{-2} is the acceleration due to gravity; $u_* = (\overline{u'w'}^2 + \overline{v'w'}^2)^{1/4}$ is the friction velocity (m s^{-1}); and $\overline{w'\theta_v'}$ is the kinematic sensible heat flux (W m^{-2}).

Reynolds decomposition for turbulent flows is applied to separate the average and fluctuating parts of the relevant quantities. The average time period used to compute the Reynolds decomposition must be much longer than any turbulence time scale, but much shorter than the time-scale for mean flow unsteadiness. For this purpose, it has been fixed to 30 minutes, a typical

time range used to compute turbulent averages for atmospheric boundary layer phenomena (De Franceschi and Zardi, 2003; De Franceschi et al., 2009; Babić et al., 2012).

As to atmospheric stability, we consider neutral atmosphere for $L \leq -500$ and $L > 500$; unstable conditions for $-500 < L \leq 0$; and stable conditions for $0 < L \leq 500$ (Muñoz-Esparza et al., 2012).

3 Wake characterization algorithm for multiple wakes

Line-of-sight velocity (u_{LOS}) measured by the WINCDUBE 200S scanning lidar (Figure 3) during the horizontal (PPI) scans can be analyzed to determine wake characteristics and how they evolve in space as the wakes propagate. Aitken et al. (2014a) proposed a wake detection algorithm and applied it to characterize the wake from a single turbine, and later expanded it to treat nacelle-based lidar measurements (Aitken and Lundquist, 2014). Here we expand the same algorithm to characterize wakes from a row of four turbines.

3.1 Data pre-processing

First, all measurements with carrier-to-noise ratio $CNR < -27$ dB are discarded from further analysis.

Moreover, in each scan, data which are not included in the interval $(\mu - 3\hat{\sigma}, \mu + 3\hat{\sigma})$ are removed from the analysis. The standard deviation $\hat{\sigma}$ is evaluated according to the median absolute deviation (MAD) In the remaining part of the wake detection algorithm, measurements will be weighted according to the inverse of the square of the radial wind speed dispersion, which is a measurement of the standard deviation of the back-scattered signal of the lidar and thus an indicator of the uncertainty of values (Vanderwende et al., 2015).

3.2 Wake detection

To implement the wake detection, measurements of line-of-sight velocity u_{LOS} at each range gate in each PPI scan are fitted to two different models: the first is for ambient flow conditions without wakes, the second represents each of the four wakes as a Gaussian function subtracted from uniform ambient flow (Tennekes and Lumley, 1972; Troldborg et al., 2007; Chamorro and Porté-Agel, 2009; Gaumond et al., 2014). Ambient wind speed is modeled with uniform speed u and direction ϕ, as shown in Figure 3. Line-of-sight velocity u_{LOS} can be related to uniform ambient wind speed u with a simple geometric transformation involving horizontal wind direction ϕ and the lidar azimuth angle α, namely:

$$u_{LOS} = u \cdot \cos(\alpha - \phi) \tag{2}$$

where both α and ϕ are > 0 for clockwise rotations. The azimuth angle α can be related to the range gate r and the transverse coordinate $y = r \cdot \cos(\theta) \cdot \sin(\alpha)$, yielding:

$$u_{LOS}(y, r) = u \cdot \left(\frac{\sqrt{r^2 - y^2}}{r} \cos\phi + \frac{y}{r} \sin\phi \right) \tag{3}$$
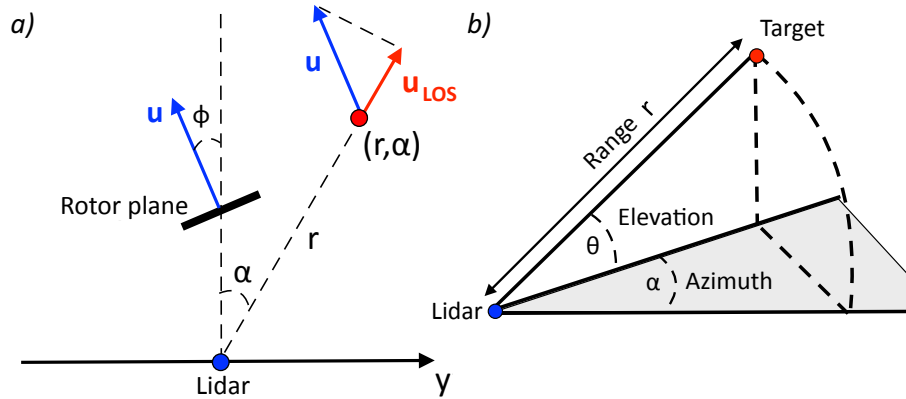
Figure 3. a) Plan view of the coordinate system for scanning lidar PPI scans. b) 3-D sketch of the main geometric quantities relevant in a lidar scan.

which represents the first model for u_{LOS} applied in the wake detection algorithm. In this case, ambient flow wind speed u and ambient wind direction ϕ are the fitting parameters of the model. This "no wake" fit is the same as in Aitken et al. (2014a). The second implemented model represents each wake from the four turbines in the row as a Gaussian function (Tennekes and Lumley, 1972) subtracted from uniform ambient flow u:

$$u_{LOS}(y,r) = \left\{ u - \sum_{i=1}^{4} a_i \exp\left[-\frac{(y-y_i)^2}{2s_{wi}^2} \right] \right\} \cdot$$
$$\cdot \left(\frac{\sqrt{r^2 - y^2}}{r} \cos\phi + \frac{y}{r} \sin\phi \right) \tag{4}$$

This second model has 14 fitting parameters: the ambient wind direction ϕ, the ambient wind speed u, the amplitudes of the Gaussian functions (i.e. the wake velocity deficit amplitudes) a_i, the four transverse coordinates of wake centers y_i, and four parameters controlling the widths of the wakes s_{wi}. Note that each of the four wakes is modeled with its own parameters, permitting variable characteristics between the wakes. The amplitude a_i can be 0, for the trivial case of no wake.

Nonlinear regression (least squares) is applied with the two different models specified above. In the fitting procedure, the transverse coordinate y is used as independent variable, while the measured line-of-sight velocity u_{LOS} is the dependent variable; moreover, the dispersion of measured u_{LOS} is used as weights for the data. In setting the first-guess values for the parameters, physical limits are set: the velocity deficit amplitudes must be ≥ 0 but lower than the uniform ambient flow wind speed u; the locations of the centers of the wakes must be included in the range of transverse coordinates y in each scan; the width of the wakes must be > 0.

The best estimates for the parameters of the two models are found. An extra sum-of-squares F test is applied to determine if the second model, which is naturally suited to better fit data considering its higher number of parameters, is *significantly* better than first model in fitting the data. A threshold p value is set to 0.05; if the calculated p value is less than this threshold, then the second model is considered capable to *significantly* better represent the data, and thus it is selected (Kleinbaum et al., 2013).
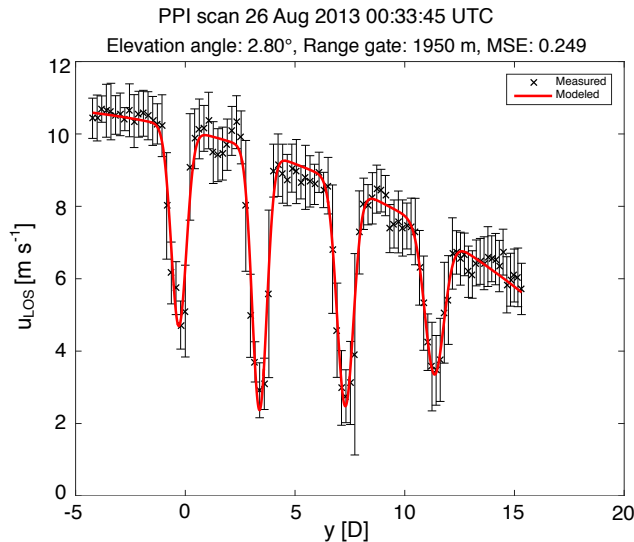
Figure 4. Example of line-of-sight velocity data measured by the scanning lidar at a specific range gate during a PPI scan. Error bars are the dispersion of line-of-sight velocity measurements. The red line represents the fit performed by the wake characterization algorithm.

Figure 4 shows an example of line-of-sight velocity measurements at a single range gate in a PPI scan (with error bars representing the dispersion of the measurements). The red continuous line is the fit performed by the wake characterization algorithm.

3.3 Model acceptance criteria

5   The quality controls implemented in the first steps of the wake detection algorithm (limits to CNR, MAD method to discard outliers, physical limits to the values of the fit parameters) assure a very good quality of the fits, measured in terms of Pearson correlation coefficient and mean squared error. However, some other quality-control steps are applied, to solve possible issues related with the complexity of the expansion of the algorithm to detect multiple wakes.

  At the smallest range gates, depending on a given wind direction, not all the four wakes from the studied row of four turbines

10   may be included in the lidar scan because of the limited range of azimuths of each scan. In these situations, the application of the second model, which aims at fitting u_{LOS} with four wakes, may result in the detection of some spurious wakes besides the actual (but less than four) real wakes seen in the PPI scan. These spurious wakes are typically detected where sudden - but very limited - natural changes in the line-of-sight velocity occur. To solve this false detection, fitted wakes with non-realistic velocity deficits (smaller than half of the minimum velocity deficits of the other wakes detected at the same range gate) and/or

15   widths (smaller than $0.1D$ or bigger than $1/4$ of the whole transverse range) are excluded from the results.

  Another issue is related to the possibility for the algorithm to detect wakes with a double-peaked shape - typical of near-wake (Magnusson, 1999), or arising from the interference of an obstacle with the laser beam of the lidar - as two separate wakes. The algorithm detects a double-peaked wake when the transverse positions of the centers of two adjacent wakes are closer

than half of the width of the largest wake. When these double-peaked wakes are detected, the algorithm can instead consider a single-peaked wake with a velocity deficit amplitude which is the average of the two detected velocity deficit amplitudes, a wake center located at the average y between the two detected peaks, and a wake width determined adding a half-width ($= 2s_{wi}$) to each external edge of the two detected peaks.

5   Besides these quality-control steps, the algorithm can re-order the remaining wake parameters, to associate them to the correct physical wake from the considered row of four turbines. This procedure is dependent on wind direction, that determines in which order the four wakes are excluded from the scan area of the lidar at lower range gates.

The wake characteristics database, resulting as output of the application of the wake detection algorithm (which is publicly available at https://github.com/nicolabodini/CWEX13), is then used to study how wake characteristics evolve in 3-dimensional

10   space.

For each detected wake, the velocity deficit is calculated as the ratio between the velocity deficit amplitude a_i and the ambient flow wind speed u (Vermeer et al., 2003):

$$VD_i = \frac{u - u_{wake}}{u} \cdot 100 = \frac{a_i}{u} \cdot 100 \tag{5}$$

The wake width has been defined in different ways in the literature; here we calculate it as in Hansen et al. (2012):

15    $$w_i = 4 \cdot s_{wi} \tag{6}$$

which is equivalent to the 95% confidence interval of the Gaussian velocity deficit profile.

The wake centerline will be studied considering the temporal evolution of the planar coordinates of the center of each wake, i.e. the peak of the velocity deficit.

As final quality-control steps, the median absolute deviation (MAD) method is applied again to discard wake characteristics

20   which do not lie within three standard deviations of the mean characteristic (Aitken et al., 2014a); moreover, only fits with Pearson correlation coefficient larger than 0.9 and mean squared error lower than 0.5 are included in the final analysis of the results.

4   Results

Once all the fits are completed, and the wakes fully characterized, it is possible to study how the wake characteristics vary in

25   space for the four studied turbines.

4.1   Frequency of wake detection and atmospheric stability

Atmospheric stability has a major impact (Churchfield et al., 2012; Iungo et al., 2013) on wind turbine wake evolution and wind farm performance: wakes in stable conditions persist for long distances downwind, while during unstable conditions the enhanced turbulent mixing erodes the wakes more quickly.

30   To get a quantitative measurement of this effect, Figure 5 shows the percentage of scans where wakes were detected by the
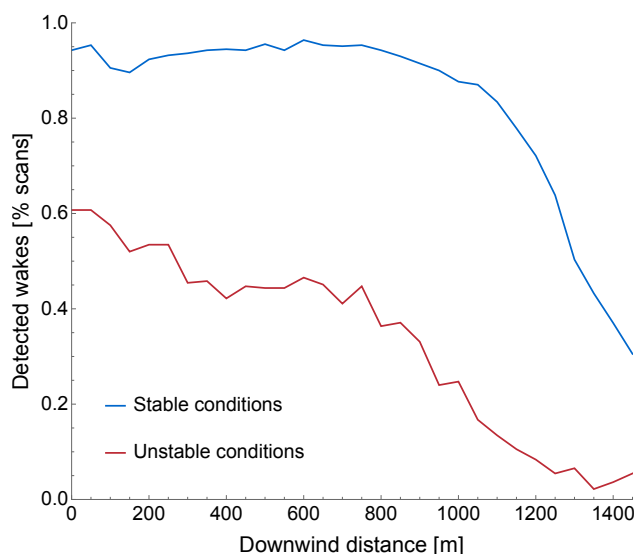
Figure 5. Percentage of wakes which are detected by the characterization algorithm vs downwind distance, for stable and unstable conditions of the atmosphere. Results from PPI scans performed on 23 and 26 August 2013.

algorithm, at each range gate, for different stability conditions of the atmosphere (measured in terms of the Obukhov Length) during 23 and 26 August 2013. The plot clearly shows how wakes can easily be detected in stable conditions, while during unstable conditions the algorithm is not capable of properly detecting wakes at least 40% of the times. Moreover, wakes erode more quickly during unstable conditions, with the degradation becoming more intense approximately at 700 m ($\sim 8.5D$)

5   downwind of the wind turbines, while under stable conditions wakes are detected in most of the scans up to approximately 1000 m ($\sim 12D$) downwind of the turbines. The results obtained are comparable for the two considered days: wind direction does not affect this result.

All the results presented in the next paragraphs focus on stable conditions of the atmosphere.

4.2   Velocity deficit results

10   Wind speed reduction in the wake region, measured in terms of velocity deficit, is the most distinct wake effect. Figure 6 shows contour plots of velocity deficits for a wake from an outer turbine (panel a) and a wake from an inner turbine (panel b), computed using the results of the wake detection algorithm from PPI scans performed at six different elevation angles from 05:31 to 05:42 UTC (from 00:31 to 00:42 LDT), 26 August 2013. The horizontal axis shows the downwind distance from the turbines, expressed in terms of rotor diameters D, with $D = 80$ m. The plot clearly shows that the velocity deficit decreases

15   with downwind distance, and the wake of the outer turbine exhibits smaller velocity deficits compared to the wake of the inner turbine.

To understand if the results are systematic, Figure 7 shows velocity deficit versus downwind distance from the turbines, calculated from the 276 PPI scans performed during the whole night (stable conditions) of 26 August 2013. The continuous lines
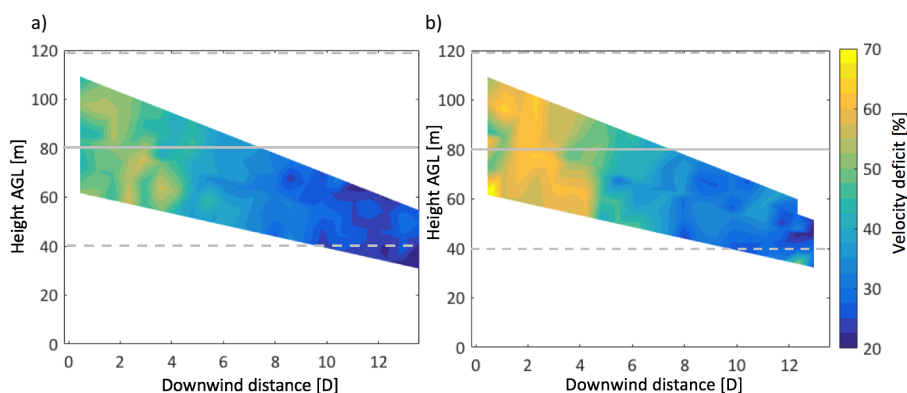
Figure 6. Velocity deficit *vs* downwind distance, at different vertical positions, for wakes from a) an outer turbine and b) an inner turbine. Gray horizontal dashed lines represent the vertical limits of the rotor disk of the turbines; the horizontal continuous gray line shows the hub height of the turbines. Data collected from 5:31 to 5:42 UTC (from 00:31 to 00:42 LDT), 26 August 2013, from a succession of six PPI scans performed at six different elevation angles.
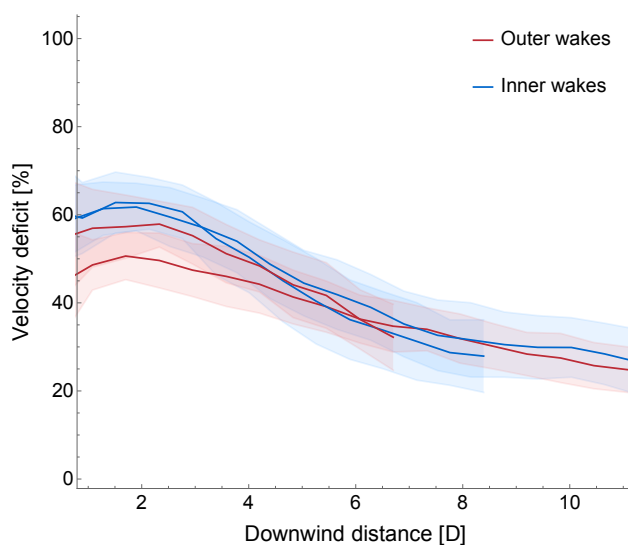
Figure 7. Velocity deficit *vs* downwind distance, for the four wakes of the studied row of turbines. Continuous lines represent the median values calculated from the 276 PPI scans performed during the night (stable conditions) of 26 August 2013; shaded areas show the standard deviation of the data.

show the median values of velocity deficit, and the shaded area represents the standard deviation of the data. As expected, velocity deficit decreases with downwind distance, since the speed reduction in the wake tends to become smaller due to the entrainment of free-stream surrounding air. The plot also confirms that wakes from outer turbines, shown in red in the plot, have lower velocity deficits than the wakes from inner turbines, for relatively low downwind distances: for one of the two outer

turbines the difference is up to 15%, while for the other it is of the order of 5%.

Comparable results occur with using data from the scans performed during the night of 23 August 2013: different wind directions do not seem to affect these results.

4.3 Wake width results

5 The widths of the wakes also change with downwind distance (expressed in terms of rotor diameters D, Figure 8). Panel $a)$ shows results from the stable conditions of the night of 26 August 2013, while panel $b)$ shows results for the stable conditions of the night of 23 August 2013. In both cases, for all the four turbines, the wake widths increase moving away from the turbine, exceeding 2 D after a downwind distance of 8-10 D.

However, if we focus on the single wakes, we can see how different wind directions (southwesterly during 26 August, south-10 easterly during 23 August) can affect the ability of the scanning lidar to measure line-of-sight velocity and, thus, detect this characteristic of the wakes. By comparing the two plots in panels $a)$ and $b)$, it is clear that the scanning lidar systematically identifies as the largest the wake which, at a given downwind distance, is more perpendicular to the laser beam (i.e. the last one the laser beam meets: turbine 4, at the right edge of the row, for southwesterly wind; turbine 1, at the left edge of the row, for southeasterly wind). Then the detected width of the wakes progressively decreases moving to the wakes from adjacent turbines.

15 Panel $c)$ in Figure 8 aggregates results from 23 and 26 August, and it shows how wake width changes with downwind distance considering the single turbines from the closest to the furthest from the scanning lidar, depending on the particular wind direction, as shown in the right schemes in the panel. The plot confirms the systematic dependence of the detected wake widths on the relative position between the wake and the scanning lidar.

4.4 Wake centerline results

20 PPI scans at multiple elevation angles provide insight into the 3-dimensional structure of wind turbine wakes. Different conditions at different vertical levels have a considerable impact on the wake centerline, i.e. the change of the position of the wake center downwind of the turbine. Figure 9 shows a plot of the median position of the centers for the wakes of the two turbines located at the west edge of the considered row of four turbines, for the 2:30 - 3:30 UTC (9:30-10:30 pm LDT) time period during the night of 26 August 2013 (southwesterly wind, panel a) and for the two turbines located at the east edge of 25 the considered row of four turbines for the 9:30 - 10:30 UTC (4:30-5:30 pm LDT) time period during the night of 23 August 2013 (southeasterly wind, panel b). Dashed lines represent the median value for the wake centerlines; continuous lines show the results for data points with different vertical heights: light colors show results for points with a vertical height between $35\,m$ and $55\,m$, dark colors refer to measurements taken above $75\,m$ AGL. A clear change in the position of the wake centers is detected between low and high vertical levels. This stretching is independent of wind direction: the change can be seen for 30 both southwesterly (panel a, 26 August) and southeasterly (panel b, 23 August) wind conditions.

This change of the wake centerline with vertical height causes a stretching of the vertical structure of the wakes: the velocity deficit structure of a turbine wake, whose stream-wise velocity deficit is traditionally considered as a 3-D Gaussian in a cross-stream plan (Figure 10 - a), should instead be represented - when this vertical stretching occurs - by a rotated ellipsoid
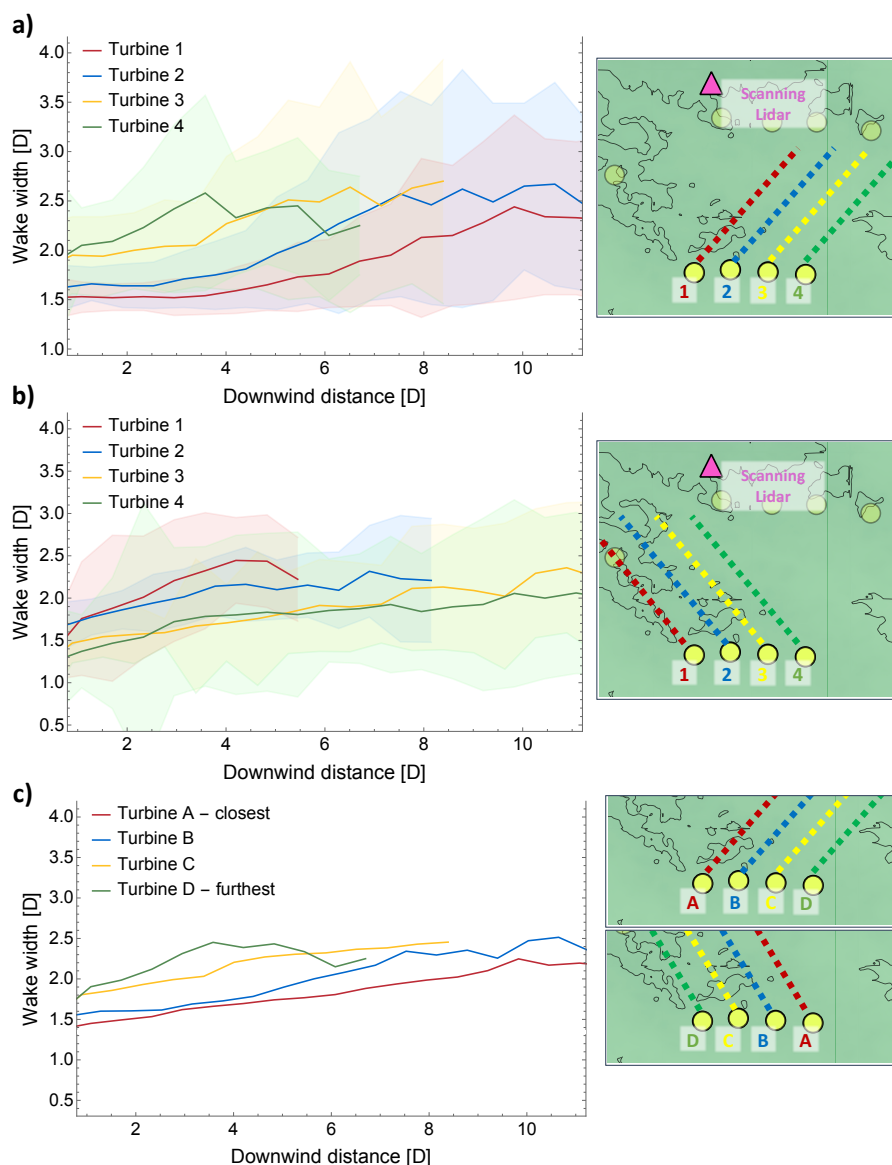
Figure 8. Wake width *vs* downwind distance from the turbines, for the wakes of the four turbines in the studied row. Continuous lines represent median values; shaded areas show the standard deviation of the data. a) Data from the night (stable conditions) of 26 August 2013, with southwesterly wind conditions. b) Data from the night (stable conditions) of 23 August 2013, with southeasterly wind conditions. c) Aggregated plot, average of data from the nights of 26 and 23 August, considering the single turbines with reference to their relative distance from the scanning lidar.

(Figure 10 - *b*), as already observed in both field measurements (Högström et al., 1988; Magnusson and Smedman, 1994) and large-eddy simulations (Lundquist et al., 2015a; Vollmer et al., 2016a).
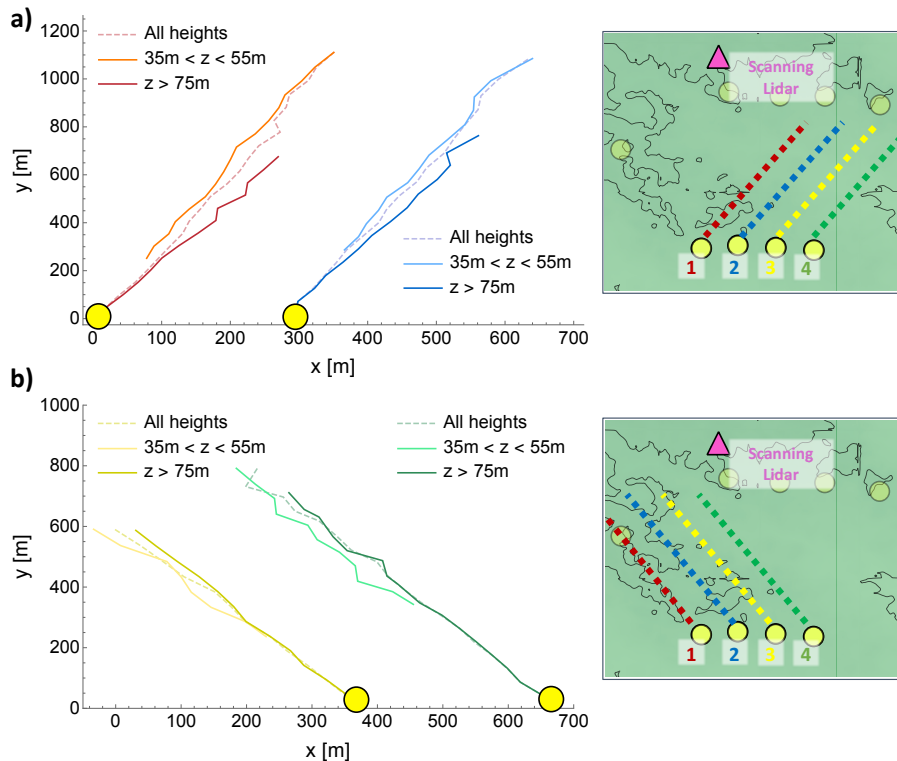
Figure 9. a) Wake centerlines for an outer (on the left) and inner (on the right) turbine, from the PPI scans measurements during the 2:30-3:30 UTC (9:30-10:30 pm LDT) time period, 26 August 2013. b) Wake centerlines for an inner (on the left) and outer (on the right) turbine, data from the 9:30-10:30 UTC (4:30-5:30 pm LDT) time period, 23 August 2013. Dashed lines represent the median values of wake centerlines, while the continuous lines show results at different vertical levels: for each wake, light colors refer to measurements between 35 m and 55 m AGL, while darker colors represent data points with a vertical height greater than 75 m. Yellow dots show the position of wind turbines.

4.4.1 Relationship between ambient veer and wake centerline

The vertical stretching of wake structure occurs because of the wind veer, the clockwise change of wind direction with height that occurs in strongly stable conditions, like those of 23 and 26 August 2013. To get a deeper insight on the relationship between ambient wind veer and vertical changes of the wake centerlines, we analyze several 30-minute periods (each corre-

5 sponding to two subsequent sequences of six PPI scans at the six different elevation angles) during the nights of 23 August 2013 (southeasterly wind) and 26 August 2013 (southwesterly wind). For each considered time frame, the wind veer is calculated as the average difference between the wind direction at $100\,m$ and $40\,m$, as measured by the vertical profiling lidar located to measure upwind conditions (WC-1 in Figure 1). The two vertical heights are chosen as representative of the two different vertical levels considered when assessing the changes of wake centerlines ($35\,\mathrm{m} < z < 55\,\mathrm{m}$ and $z > 75\,\mathrm{m}$). Moreover, the wake

10 centerlines at different vertical levels have been fitted with straight lines, and the angle between the lines which approximate the wake centerlines at $35\,\mathrm{m} < z < 55\,\mathrm{m}$ and $z > 75\,\mathrm{m}$ is calculated and then considered as the angular difference between
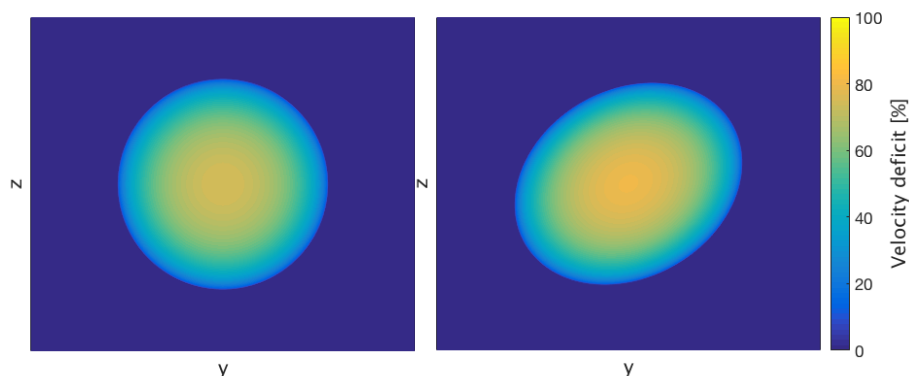
Figure 10. Qualitative cross-stream slices of stream-wise velocity deficit. The perspective is looking downwind. On the left, a graphic representation of the classical Gaussian shape of the magnitude of wake velocity deficit. On the right, an ellipsoid which represents the vertical stretching of the 3-D structure of a turbine wake as a consequence of wind veer.

the wake centerlines at different vertical levels. Figure 11 shows how angular difference between wake centerlines at different vertical levels compares to ambient wind veer between 100 m and 40 m, for all the available time frames during the nights of 23 and 26 August 2013, for wakes from an inner and an outer turbine in the considered row. The results show that, although the angular change in the wake centerline at different vertical levels is systematically detected, the wind veer is always much larger than the actual angular difference between the wake centerlines at the different vertical levels: the change of the positions of the wake centers is related to, but not completely determined by, the wind veer. Moreover, wakes from outer turbines often present a larger angular difference in wake centerlines compared to wakes from inner turbines, as shown by the linear regression fits.

5 Conclusions

Wakes from a row of four turbines have been characterized using line-of-sight wind speed measurements from PPI scans performed by a scanning lidar. Data were collected in late summer 2013 during the CWEX-13 field campaign (Lundquist et al., 2014), in a wind farm in a flat region in central Iowa. The wake characterization algorithm proposed by Aitken et al. (2014a) has been extended to assess wakes from multiple turbines.

Wakes erode quickly during unstable conditions of the atmosphere, and they can in fact be detected here primarily in stable conditions in this dataset. The velocity deficit in the wakes decreases with downwind distance from the turbines, and it is lower for wakes from outer turbines in the studied row. The width of the wakes increases with downwind distance, with systematic differences in the ability of the scanning lidar to detect the width of the wake according to the component of the direction the wakes perpendicular to the direction of laser beam of the scanning lidar. Wake centerlines change at different vertical levels as a consequence of the ambient wind veer, causing a stretching of the vertical structure of the wakes. Although the field measurements of Högström et al. (1988); Magnusson and Smedman (1994) demonstrated that turbine wakes stretch into ellipses during stable conditions, for the first time we have quantified the effect of ambient wind veer on the stretching of
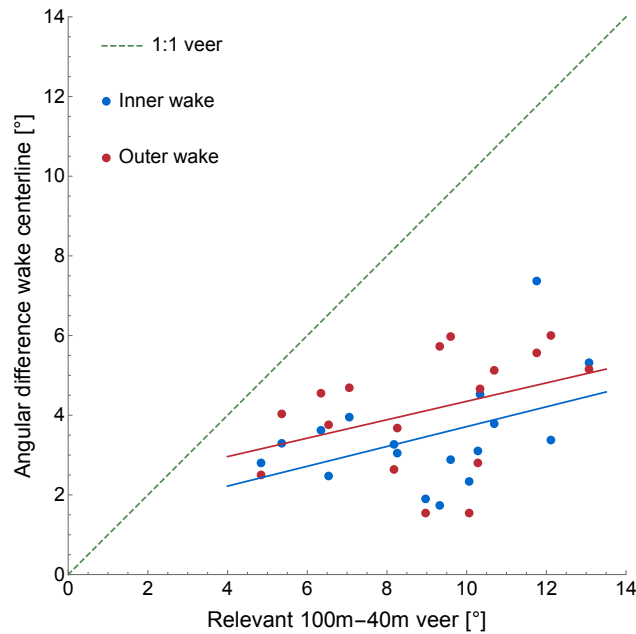
Figure 11. Angular difference between wake centerlines at different vertical heights ($35\ \text{m} < z < 55\ \text{m}$ and $z > 75\ \text{m}$) *vs* wind veer between 100 m and 40 m. Data for an inner and an outer wake in the considered row of 4 turbines, for several 30-minutes time frames during the nights of 23 and 26 August 2013. Continuous lines are the linear regressions from the data (red best-fit: $2.04+0.23x$, blue best-fit: $1.23+0.25x$), for the outer and the inner wake. Dashed line highlights the not-reached equality between ambient veer and wake centerlines angular difference.

wakes. In fact, the angular change in the wake centerlines at different heights is systematically much lower (a half or less) than the wind veer registered at the same heights. Moreover, this angular change of the wake centerlines at different vertical levels is found to be usually greater for wakes from outer turbines. This wake stretching, due to wind veer, is not only seen in these field measurements but also emerges in the stably-stratified simulations of Aitken et al. (2014b); Bhaganagar and Debnath

5 (2015); Lundquist et al. (2015b); Vollmer et al. (2016b); Abkar et al. (2016). As more three-dimensional measurements of wakes become available due to the use of scanning lidar and scanning radar, a more solid representation of wind turbine wakes can be assessed.

These results can become critically important to assess and improve large-eddy simulations of wakes as well as to suggest improvements to mesoscale parametrizations (Fitch et al., 2012, 2013; Jiménez et al., 2015; Lee and Lundquist, 2017) to

10 account for subgridscale wake interactions. Moreover, wind energy companies can also benefit from our results in trying to enhance the quality of low-order wake models currently used for wind resource assessment, wind farm layout optimization and wind farm control techiniques, with the final goal of an improvement of wind energy production efficiency.

6 Code availability

The Matlab code of the wake characterization algorithm is publicly available at https://github.com/nicolabodini/CWEX13.

7 Data availability

CWEX-13 data will be publicly-available at the Dept. of Energy Atmosphere to electrons archive at https://a2e.energy.gov/projects.

5 *Acknowledgements.* This work was partially supported by the National Renewable Energy Laboratory under APUP UGA-0-41026-22 and by the National Science Foundation grant BCS-1413980 (Coupled Human Natural Systems). Nicola Bodini was partiallly supported by a grant from the University of Trento for a visit to the University of Colorado Boulder in summer 2016.

References

Abkar, M. and Porté-Agel, F.: Influence of atmospheric stability on wind-turbine wakes: A large-eddy simulation study, Physics of Fluids, 27, 035 104, 2015.

Abkar, M., Sharifi, A., and Porté-Agel, F.: Large-eddy simulation of the diurnal variation of wake flows in a finite-size wind farm, in: Journal of Physics: Conference Series, vol. 625, p. 012031, IOP Publishing, 2015.

Abkar, M., Sharifi, A., and Porté-Agel, F.: Wake flow in a wind farm during a diurnal cycle, Journal of Turbulence, 17, 420–441, doi:10.1080/14685248.2015.1127379, 2016.

Aitken, M. L. and Lundquist, J. K.: Utility-scale wind turbine wake characterization using nacelle-based long-range scanning lidar, Journal of Atmospheric and Oceanic Technology, 31, 1529–1539, doi:10.1175/JTECH-D-13-00218.1, 2014.

Aitken, M. L., Banta, R. M., Pichugina, Y. L., and Lundquist, J. K.: Quantifying wind turbine wake characteristics from scanning remote sensor data, Journal of Atmospheric and Oceanic Technology, 31, 765–787, doi:10.1175/JTECH-D-13-00104.1, 2014a.

Aitken, M. L., Kosović, B., Mirocha, J. D., and Lundquist, J. K.: Large eddy simulation of wind turbine wake dynamics in the stable boundary layer using the Weather Research and Forecasting Model, Journal of Renewable and Sustainable Energy, 6, 033 137, doi:10.1063/1.4885111, 2014b.

Andersen, S. J., Sørensen, J. N., Ivanell, S., and Mikkelsen, R. F.: Comparison of engineering wake models with CFD simulations, in: Journal of physics: Conference series, vol. 524, p. 012161, IOP Publishing, 2014.

Aubrun, S., Garcia, E. T., Boquet, M., Coupiac, O., and Girard, N.: Wind turbine wake tracking and its correlations with wind turbine monitoring sensors. Preliminary results, in: Journal of Physics: Conference Series, vol. 753, p. 032003, IOP Publishing, 2016.

Babić, K., Bencetić Klaić, Z., and Večenaj, Ž.: Determining a turbulence averaging time scale by Fourier analysis for the nocturnal boundary layer, Geofizika, 29, 35–51, 2012.

Banta, R. M., Pichugina, Y. L., Brewer, W. A., Lundquist, J. K., Kelley, N. D., Sandberg, S. P., Alvarez II, R. J., Hardesty, R. M., and Weickmann, A. M.: 3D volumetric analysis of wind turbine wake properties in the atmosphere using high-resolution Doppler lidar, Journal of Atmospheric and Oceanic Technology, 32, 904–914, 2015.

Barthelmie, R., Larsen, G., Frandsen, S., Folkerts, L., Rados, K., Pryor, S., Lange, B., and Schepers, G.: Comparison of wake model simulations with offshore wind turbine wake profiles measured by sodar, Journal of atmospheric and oceanic technology, 23, 888–901, 2006.

Barthelmie, R. J., Pryor, S., Frandsen, S. T., Hansen, K. S., Schepers, J., Rados, K., Schlez, W., Neubert, A., Jensen, L., and Neckelmann, S.: Quantifying the impact of wind turbine wakes on power output at offshore wind farms, Journal of Atmospheric and Oceanic Technology, 27, 1302–1317, 2010.

Barthelmie, R. J., Hansen, K. S., and Pryor, S. C.: Meteorological controls on wind turbine wakes, Proceedings of the IEEE, 101, 1010–1019, 2013.

Bastine, D., Wächter, M., Peinke, J., Trabucchi, D., and Kühn, M.: Characterizing Wake Turbulence with Staring Lidar Measurements, J. Phys.: Conf. Ser., 625, 012 006, doi:10.1088/1742-6596/625/1/012006, 2015.

Bhaganagar, K. and Debnath, M.: The effects of mean atmospheric forcings of the stable atmospheric boundary layer on wind turbine wake, Journal of Renewable and Sustainable Energy, 7, 013 124, doi:10.1063/1.4907687, 2015.

Bingöl, F., Mann, J., and Larsen, G. C.: Light detection and ranging measurements of wake dynamics part I: one-dimensional scanning, Wind Energy, 13, 51–61, doi:10.1002/we.352, 2010.

Brower, M.: Wind resource assessment: a practical guide to developing a wind project, John Wiley & Sons, 2012.

Chamorro, L. P. and Porté-Agel, F.: A Wind-Tunnel Investigation of Wind-Turbine Wakes: Boundary-Layer Turbulence Effects, Boundary-Layer Meteorology, 132, 129–149, doi:10.1007/s10546-009-9380-8, 2009.

Chowdhury, S., Zhang, J., Messac, A., and Castillo, L.: Unrestricted wind farm layout optimization (UWFLO): Investigating key factors influencing the maximum power generation, Renewable Energy, 38, 16–30, 2012.

5   Churchfield, M. J., Lee, S., Michalakes, J., and Moriarty, P. J.: A numerical study of the effects of atmospheric and wake turbulence on wind turbine dynamics, Journal of turbulence, p. N14, 2012.

Clifton, A., Smith, A., and Fields, M.: Wind Plant Preconstruction Energy Estimates: Current Practice and Opportunities, Tech. rep., NREL (National Renewable Energy Laboratory (NREL), Golden, CO (United States)), http://www.nrel.gov/docs/fy16osti/64735.pdf, 2016.

Clive, P. J., Dinwoodie, I., and Quail, F.: Direct measurement of wind turbine wakes using remote sensing, Proc. EWEA 2011, 2011.

10 Crespo, A., Hernandez, J., and Frandsen, S.: Survey of modelling methods for wind turbine wakes and wind farms, Wind energy, 2, 1–24, 1999.

De Franceschi, M. and Zardi, D.: Evaluation of cut-off frequency and correction of filter-induced phase lag and attenuation in eddy covariance analysis of turbulence data, Boundary-layer meteorology, 108, 289–303, 2003.

De Franceschi, M., Zardi, D., Tagliazucca, M., and Tampieri, F.: Analysis of second-order moments in surface layer turbulence in an Alpine
15   valley, Quarterly Journal of the Royal Meteorological Society, 135, 1750–1765, 2009.

Dörenkämper, M., Witha, B., Steinfeld, G., Heinemann, D., and Kühn, M.: The impact of stable atmospheric boundary layers on wind-turbine wakes within offshore wind farms, Journal of Wind Engineering and Industrial Aerodynamics, 144, 146–153, doi:10.1016/j.jweia.2014.12.011, 2015.

Elkinton, C. N., Manwell, J. F., and McGowan, J. G.: Offshore wind farm layout optimization (OWFLO) project: Preliminary results,
20   University of Massachusetts, 2006.

Fitch, A. C., Olson, J. B., Lundquist, J. K., Dudhia, J., Gupta, A. K., Michalakes, J., and Barstad, I.: Local and Mesoscale Impacts of Wind Farms as Parameterized in a Mesoscale NWP Model, Monthly Weather Review, 140, 3017–3038, doi:10.1175/MWR-D-11-00352.1, 2012.

Fitch, A. C., Olson, J. B., and Lundquist, J. K.: Parameterization of Wind Farms in Climate Models, Journal of Climate, 26, 6439–6458, doi:10.1175/JCLI-D-12-00376.1, 2013.

25 Fleming, P. A., Gebraad, P. M., Lee, S., van Wingerden, J.-W., Johnson, K., Churchfield, M., Michalakes, J., Spalart, P., and Moriarty, P.: Evaluating techniques for redirecting turbine wakes using SOWFA, Renewable Energy, 70, 211–218, 2014.

Fleming, P. A., Ning, A., Gebraad, P. M. O., and Dykes, K.: Wind plant system engineering through optimization of layout and yaw control, Wind Energ., 19, 329–344, doi:10.1002/we.1836, 2016.

Gaumond, M., Réthoré, P.-E., Ott, S., Pena, A., Bechmann, A., and Hansen, K. S.: Evaluation of the wind direction uncertainty and its impact
30   on wake modeling at the Horns Rev offshore wind farm, Wind Energy, 17, 1169–1178, 2014.

Gebraad, P., Teeuwisse, F., Wingerden, J., Fleming, P. A., Ruben, S., Marden, J., and Pao, L.: Wind plant power optimization through yaw control using a parametric model for wake effects—a CFD simulation study, Wind Energy, 19, 95–114, 2016.

Hansen, K. S., Barthelmie, R. J., Jensen, L. E., and Sommer, A.: The impact of turbulence intensity and atmospheric stability on power deficits due to wind turbine wakes at Horns Rev wind farm, Wind Energy, 15, 183–196, 2012.

35 Hirth, B. D. and Schroeder, J. L.: Documenting Wind Speed and Power Deficits behind a Utility-Scale Wind Turbine, Journal of Applied Meteorology and Climatology, 52, 39–46, doi:10.1175/JAMC-D-12-0145.1, 2013.

Hirth, B. D., Schroeder, J. L., Gunter, W. S., and Guynes, J. G.: Measuring a utility-scale turbine wake using the TTUKa mobile research radars, Journal of Atmospheric and Oceanic Technology, 29, 765–771, 2012.

Högström, U., Asimakopoulos, D., Kambezidis, H., Helmis, C., and Smedman, A.: A field study of the wake behind a 2 MW wind turbine, Atmospheric Environment (1967), 22, 803–820, 1988.

Iungo, G. V., Wu, Y.-T., and Porté-Agel, F.: Field Measurements of Wind Turbine Wakes with Lidars, Journal of Atmospheric and Oceanic Technology, 30, 274–287, doi:10.1175/JTECH-D-12-00051.1, 2013.

5 Jensen, N. O., Petersen, E. L., and Troen, I.: Extrapolation of Mean Wind Statistics with Special Regard to Wind Energy Applications., Tech. rep., 1984.

Jiménez, P. A., Navarro, J., Palomares, A. M., and Dudhia, J.: Mesoscale modeling of offshore wind turbine wakes at the wind farm resolving scale: a composite-based analysis with the Weather Research and Forecasting model over Horns Rev, Wind Energ., 18, 559–566, doi:10.1002/we.1708, 2015.

10 Käsler, Y., Rahm, S., Simmet, R., and Kühn, M.: Wake measurements of a multi-MW wind turbine with coherent long-range pulsed Doppler wind lidar, Journal of Atmospheric and Oceanic Technology, 27, 1529–1532, 2010.

Kleinbaum, D. G., Kupper, L. L., Nizam, A., and Rosenberg, E. S.: Applied regression analysis and other multivariable methods, Nelson Education, 2013.

Kumer, V.-M., Reuder, J., Svardal, B., Sætre, C., and Eecen, P.: Characterisation of single wind turbine wakes with static and scanning

15 WINTWEX-W LiDAR data, Energy Procedia, 80, 245–254, 2015.

Landberg, L.: Meteorology for Wind Energy: An Introduction, John Wiley & Sons, 2015.

Lee, J. C.-Y. and Lundquist, J.: Observing and Simulating Wind Turbine Wakes during the Evening Transition, Boundary-Layer Meteorology, in review, 2017.

Lundquist, J., Churchfield, M., Lee, S., and Clifton, A.: Quantifying error of lidar and sodar Doppler beam swinging measurements of wind

20 turbine wakes using computational fluid dynamics, Atmospheric Measurement Techniques, 8, 907–920, 2015a.

Lundquist, J. K., Takle, E. S., Boquet, M., Kosović, B., Rhodes, M. E., Rajewski, D., Doorenbos, R., Irvin, S., Aitken, M. L., Friedrich, K., et al.: Lidar observations of interacting wind turbine wakes in an onshore wind farm, in: EWEA meeting proceedings, 2014.

Lundquist, J. K., Churchfield, M. J., Lee, S., and Clifton, A.: Quantifying error of lidar and sodar Doppler beam swinging measurements of wind turbine wakes using computational fluid dynamics, Atmos. Meas. Tech., 8, 907–920, doi:10.5194/amt-8-907-2015, 2015b.

25 Machefaux, E., Larsen, G. C., Koblitz, T., Troldborg, N., Kelly, M. C., Chougule, A., Hansen, K. S., and Rodrigo, J. S.: An experimental and numerical study of the atmospheric stability impact on wind turbine wakes, Wind Energy, 2015.

Magnusson, M.: Near-wake behaviour of wind turbines, Journal of Wind Engineering and Industrial Aerodynamics, 80, 147–167, 1999.

Magnusson, M. and Smedman, A.: Influence of atmospheric stability on wind turbine wakes, Wind Engineering, 18, 139–152, 1994.

Mirocha, J. D., Kosovic, B., Aitken, M. L., and Lundquist, J. K.: Implementation of a generalized actuator disk wind turbine model into the

30 weather research and forecasting model for large-eddy simulation applications, Journal of Renewable and Sustainable Energy, 6, 013 104, doi:10.1063/1.4861061, 2014.

Mirocha, J. D., Rajewski, D. A., Marjanovic, N., Lundquist, J. K., Kosović, B., Draxl, C., and Churchfield, M. J.: Investigating wind turbine impacts on near-wake flow using profiling lidar data and large-eddy simulations with an actuator disk model, Journal of Renewable and Sustainable Energy, 7, 043 143, 2015.

35 Muñoz-Esparza, D., Cañadillas, B., Neumann, T., and van Beeck, J.: Turbulent fluxes, stability and shear in the offshore environment: Mesoscale modelling and field observations at FINO1, Journal of Renewable and Sustainable Energy, 4, 063 136, doi:10.1063/1.4769201, 2012.

Nygaard, N. G.: Wakes in very large wind farms and the effect of neighbouring wind farms, in: Journal of Physics: Conference Series, vol. 524, p. 012162, IOP Publishing, 2014.

Rajewski, D. A., Takle, E. S., Lundquist, J. K., Oncley, S., Prueger, J. H., Horst, T. W., Rhodes, M. E., Pfeiffer, R., Hatfield, J. L., Spoth, K. K., and Doorenbos, R. K.: CROP WIND ENERGY EXPERIMENT (CWEX): Observations of Surface-Layer, Boundary Layer, and Mesoscale Interactions with a Wind Farm, Bulletin of the American Meteorological Society, 94, 655–672, http://0-search.proquest.com.libraries.colorado.edu/docview/1368160232/abstract/2AD773836C1B4F73PQ/1, 2013.

Rhodes, M. E. and Lundquist, J. K.: The Effect of Wind-Turbine Wakes on Summertime US Midwest Atmospheric Wind Profiles as Observed with Ground-Based Doppler Lidar, Boundary-Layer Meteorology, 149, 85–103, doi:10.1007/s10546-013-9834-x, 2013.

Samorani, M.: The wind farm layout optimization problem, in: Handbook of Wind Power Systems, pp. 21–38, Springer, 2013.

Sathe, A. and Mann, J.: A review of turbulence measurements using ground-based wind lidars, Atmospheric Measurement Techniques, 6, 3147–3167, doi:10.5194/amt-6-3147-2013, http://www.atmos-meas-tech.net/6/3147/2013/, 2013.

Sathe, A., Mann, J., Barlas, T., Bierbooms, W., and van Bussel, G.: Influence of atmospheric stability on wind turbine loads: Atmospheric stability and loads, Wind Energy, 16, 1013–1032, doi:10.1002/we.1528, http://doi.wiley.com/10.1002/we.1528, 2013.

Spera, D.: Method for evaluating wind turbine wake effects on wind farm performance, Journal of Solar Energy Engineering, 107, 241, 1985.

Takle, E. S., Rajewski, D. A., Lundquist, J. K., Jr, W. A. G., and Sharma, A.: Measurements in support of wind farm simulations and power forecasts: The Crop/Wind-energy Experiments (CWEX), J. Phys.: Conf. Ser., 524, 012 174, doi:10.1088/1742-6596/524/1/012174, 2014.

Tennekes, H. and Lumley, J. L.: A first course in turbulence, MIT press, 1972.

Troldborg, N., Sørensen, J. N., and Mikkelsen, R.: Actuator line simulation of wake of wind turbine operating in turbulent inflow, in: Journal of physics: conference series, vol. 75, p. 012063, IOP Publishing, 2007.

Trujillo, J.-J., Bingöl, F., Larsen, G. C., Mann, J., and Kühn, M.: Light detection and ranging measurements of wake dynamics. Part II: two-dimensional scanning, Wind Energy, 14, 61–75, 2011.

Vanderwende, B. J. and Lundquist, J. K.: The modification of wind turbine performance by statistically distinct atmospheric regimes, Environmental Research Letters, 7, 034 035, doi:10.1088/1748-9326/7/3/034035, 2012.

Vanderwende, B. J., Lundquist, J. K., Rhodes, M. E., Takle, E. S., and Irvin, S. L.: Observing and Simulating the Summertime Low-Level Jet in Central Iowa, Monthly Weather Review, 143, 2319–2336, doi:10.1175/MWR-D-14-00325.1, 2015.

Vermeer, L., Sørensen, J. N., and Crespo, A.: Wind turbine wake aerodynamics, Progress in aerospace sciences, 39, 467–510, 2003.

Vollmer, L., Steinfeld, G., Heinemann, D., and Kühn, M.: Estimating the wake deflection downstream of a wind turbine in different atmospheric stabilities: an LES study, Wind Energy Science, 1, 129–141, doi:10.5194/wes-1-129-2016, http://www.wind-energ-sci.net/1/129/2016/, 2016a.

Vollmer, L., Steinfeld, G., Heinemann, D., and Kühn, M.: Estimating the wake deflection downstream of a wind turbine in different atmospheric stabilities: An LES study, Wind Energy Science, in open discussion, doi:doi:10.5194/wes-2016-4, 2016b.

Wharton, S. and Lundquist, J. K.: Atmospheric stability affects wind turbine power collection, Environmental Research Letters, 7, 014 005, doi:10.1088/1748-9326/7/1/014005, 2012.